Optimization of optical convolution kernel of optoelectronic hybrid convolution neural network[*]

XU Xiaofeng[1], ZHU Lianqing[1,2]**, ZHUANG Wei[2], ZHANG Dongliang[2], LU Lidan[3], and YUAN Pei[3]

1. *School of Electro-Optical Engineering, Changchun University of Science and Technology, Jilin 130022, China*
2. *Key Laboratory of the Ministry of Education for Optoelectronic Measurement Technology and Instrument, Beijing Information Science and Technology University, Beijing 100192, China*
3. *Beijing Laboratory of Optical Fiber Sensing and System, Beijing Information Science and Technology University, Beijing 100016, China*

To enhance the optical computation's utilization efficiency, we develop an optimization method for optical convolution kernel in the optoelectronic hybrid convolution neural network (OHCNN). To comply with the actual calculation process, the convolution kernel is expanded from single-channel to two-channel, containing positive and negative weights. The Fashion-MNIST dataset is used to test the network architecture's accuracy, and the accuracy is improved by 7.5% with the optimized optical convolution kernel. The energy efficiency ratio (*EER*) of two-channel network is 46.7% higher than that of the single-channel network, and it is 2.53 times of that of traditional electronic products.

Fast and low-power image recognition technology is essential in unmanned mobile devices. Convolution neural network (CNN) can deal with the variability of two-dimensional (2D) shapes and is widely used in image analysis of unmanned mobile devices[1,2]. Although graphics processing unit (GPU) accelerator, field programmable gate array (FPGA), and other unique customized electronic architectures for CNN have made significant progress, large matrix multiplication of the image and video generated by these devices consumes power overly. Reducing CNN's power consumption can extend the working time of unmanned equipment. Thus, many groups have widely developed fast and low-power platforms for CNN.

Neuromorphic photonics is an emerging field at the intersection of photonics and neuromorphic engineering. It can accelerate the processing of information and broaden the bandwidth[3]. SHEN et al[4] proposed a novel architecture for an optical neural network, which comprised an optical interference unit (OIU) and an optical nonlinearity unit (ONU). Its accuracy is 76.7%, and the power efficiency is three orders than conventional learning tasks. However, the all-optical CNN photonic neural network is difficult to realize. BANGARI et al[5] proposed a digital electronic and analog photonic scheme, suited for CNN, which is 2.8—14 times faster than a GPU with only 0.75 time of the energy consumption.

ONG et al[6] proposed a scalable architecture for photonic and electronic convolutional neural networks using the Fourier transform property of star couplers. To optimize the optoelectronic hybrid convolution neural network (OHCNN) structure, PAI et al[7] explored mesh architecture improvements to enhance these devices' training speed and scalability, such as adding extra tunable beam-splitters or permuting waveguide layers. YING et al[8] showed a more efficient architecture that uses a sparse tree network block, a single unitary block, and a diagonal block for each neural network layer. The Mach-Zehnder interferometers (MZIs) area cost is less than various sizes of optical neural networks.

In our previous work[9], the photoelectric hybrid neural network is developed. This network has an accuracy rate of 88.79%, and the energy efficiency ratio (*EER*) is 1.73 times of that of traditional electronic products. In this paper, we build an OHCNN composed of OIU and FPGA. The OIU performs multiplication and accumulation operations, which are composed of MZIs array. FPGA caches data, controls OIU, and implements nonlinear activation, simultaneously. First, the convolution kernel layer is split and reorganized. Then, it is encoded and modulated by FPGA. To maximize the optical computation's utilization efficiency, we develop an optimization method for the optical convolution kernel in the OHCNN. This method enables optical calculation's value

with both positive and negative weights. Meanwhile, an analysis framework is adopted to determine the recognition accuracy of the OHCNN and estimate the final power consumption. This method provides a fast and low-power blueprint for the real-time identification of unmanned equipment.

CNN consists of a set of successive layers of convolution, pooling, nonlinearities, and a final fully connected layer (FCL) (depicted in Fig.1(a)). Generally, CNN can be computed by forwarding propagation and then optimized with back-propagation. Convolution and pooling can be realized by linear combinations (e.g. matrix multiplication). FCL maps the convolution output to a set of classification outputs. As we know, the superposition of several small kernels reduces computational complexity when the connectivity remains unchanged. However, overly small kernels cannot represent the map's characteristics. Thus, multiple suitable kernels are chosen in convolution.
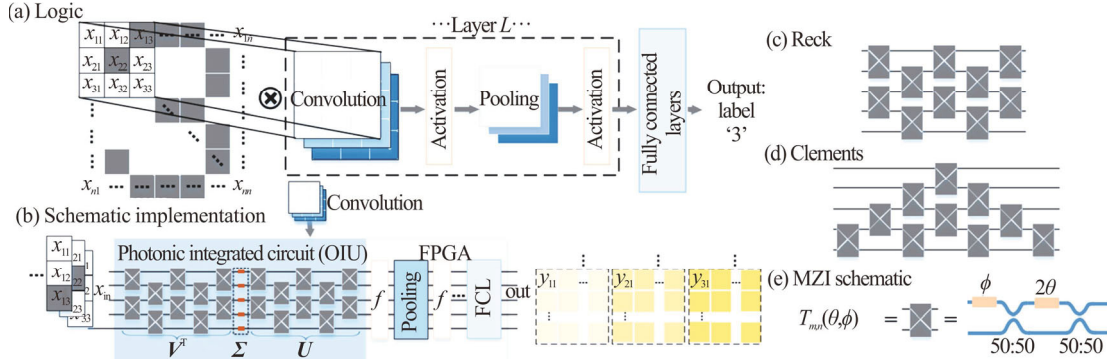
Fig.1 General architecture of OHCNN: (a) CNN operational logic; (b) OHCNN schematic implementation; Universal unitary matrix proposed by (c) RECK et al and (d) CLEMENTS et al; (e) MZI schematic

The convolution layer consists of N kernels ($N \geq 1$). Every $n_c \times n_c$ convolution kernel is a channel ($n_c \geq 1$). Computation for a single node in the output channel z_{A_1} ($A \leq N$) is shown as

$$z_{A_1} = \text{Act}((c_{A_{11}} x_{11} + c_{A_{12}} x_{12} + c_{A_{13}} x_{13} + \cdots + c_{A_{1j}} x_{1j} + \cdots +$$
$$c_{A_{i1}} x_{i1} + c_{A_{i2}} x_{i2} + c_{A_{i3}} x_{i3} + \cdots + c_{A_{ij}} x_{ij}) + b_{A_1}), \quad (1)$$

where $c_{A_{ij}}$ ($i, j = 1, 2, 3, \cdots, n_c$) is the kernel for channels A, x_{ij} ($i, j = 1, 2, 3, \cdots, n_c$) is input, and b_{A_1} is the bias.

As shown in Fig.1(b), the OHCNN consists of an OIU and an FPGA. Here, OIU implements convolution. FPGA realizes nonlinear activation, pooling and FCL, controls the OIU, encodes the input, and calls OIU repeatedly, simultaneously. The optical intensity of OIU is converted to an electrical signal by a photodetector (PD). In our previous work[9], three 3×3 kernels and rectified linear unit (ReLU) nonlinear activation function are used in each convolution layer. FCL maps the convolution output to a set of labels and selects the label with the maximum probability value as the prediction label based on probability values obtained by SOFTMAX.

OIU can implement any real-valued $m \times n$ matrix ($\mathbf{M}$). As depicted in Fig.1(b), matrix $\mathbf{M}$ can be implemented using a mesh of OIU. It can be decomposed using singular value decomposition (SVD) as

$$\mathbf{M} \rightarrow \mathbf{U\Sigma V}^{\text{T}}, \quad (2)$$

where $\mathbf{U}$ is an $m \times m$ unitary matrix, $\mathbf{V}^{\text{T}}$ is the complex conjugate of the $n \times n$ unitary matrix $\mathbf{V}$, and $\mathbf{\Sigma}$ is an $m \times n$ diagonal matrix with non-negative-real numbers on the diagonal. Any unitary matrix $\mathbf{U}$ can be decomposed into a product of $\mathbf{T}_{m,n}(\theta, \varphi)$[10,11] as

$$\mathbf{U} = \mathbf{D}(\prod_{(m,n) \in S} \mathbf{T}_{m,n}(\theta, \varphi)), \quad (3)$$

where S is a specific ordered domain belonging to (m, n). $\mathbf{D}$ is a diagonal matrix with complex elements and its modulus equal to 1 on the diagonal. An MZI can implement $\mathbf{T}_{m,n}(\theta, \varphi)$, consisting of two 50:50 directional couplers, a phase shift φ at one input port and another phase shift θ on interference arm (depicted in Fig.1(e)). $\mathbf{T}_{m,n}(\theta, \varphi)$ can be expressed as

$$\mathbf{T}_{m,n}(\theta, \varphi) = \begin{bmatrix} 1 & 0 & \cdots & & \cdots & \cdots & 0 \\ 0 & \ddots & & & & & \vdots \\ \vdots & & e^{i\varphi} \cos\theta & -\sin\theta & & \vdots \\ \vdots & & e^{i\varphi} \sin\theta & \cos\theta & & \vdots \\ \vdots & & & & \ddots & 0 \\ 0 & \cdots & \cdots & & \cdots & 0 & 1 \end{bmatrix}. \quad (4)$$

Phase shifter θ in the middle of MZI's two arms controls the splitting ratio of the output modes. Phase shifter φ in the middle of two MZIs controls the relative phase of the output mode. Here, the transformation between channels m and n ($m = n - 1$) corresponds to a lossless beam splitter between channels m and n with reflectivity $\cos\theta$ ($\theta \in [0, \pi/2]$) and a phase shift φ ($\varphi \in [0, 2\pi]$) at input m[10]. A universal n-D unitary matrix can be implemented using $n(n-1)/2$ MZIs, and the arrangement of these MZIs can be organized in Fig.1(c) proposed by RECK et al[11] or in Fig.1(d) proposed by CLEMENTS et al[10]. Optical attenuators or optical amplification materials can implement $\mathbf{\Sigma}$ operation[12].

The Fashion-MNIST is a ten-category clothing dataset, including 60 000 training sets and 10 000 testing sets. Each image in the dataset contains 28×28 pixels, and these numbers are normalized and fixed in the center. Different from the MNIST dataset, the Fashion-MNIST dataset is no longer an abstract number symbol, but a more specific clothing type. The image is compressed to 4 bits, and then 16-pulse amplitude modulation (PAM16) converts image information into optical signals. We train the matrix parameters with the stochastic gradient descent method. In the simulation state, each batch of data is 300, the number of cycles is 10, the loss function is the cross-entropy function, and the optimizer is the Adam optimizer, and the learning rate is 0.01.

To reduce MZIs in CNN and enhance the working efficiency, we develop a new decomposition method for the convolution kernel. As depicted in Fig.2(a), taking three 3×3 kernels C_i as an example, each row of the kernel C_i matches each row of the sub-image X. C_i is divided into three rows. Thus, these three convolution kernels' ith row converts into a new matrix C_i' of 3×3. Then, a linear matrix operation is executed between C_i' and the sub-image's ith row X_i. Eventually, the sub-image's characteristic matrix Y is obtained as

$$Y = \sum_{i=1}^{3} C_i' \times X_i^{\mathrm{T}}. \tag{5}$$

Each 3×3 OIU can implement a C_i'. C_i' is realized with

9 MZIs and 18 phase shifting elements (shown in Fig.2(b)). This method can realize any w $h×h$ kernels. The matrix should be padded with zero, when $w/3{\neq}0$ or $(h^2)/3{\neq}0$.

Due to the optical devices' particularity, optical computation for realizing negative number operation is limited. To maximize the efficiency of optical computing, the new convolution kernel C_i' and input X_i are expanded from single-channel to two-channel, which contains positive and negative information, respectively (depicted in Fig.2(a)).

$$Y = \sum_{i=1}^{3} C_i' \times X_i^{\mathrm{T}} = \sum_{i=1}^{3} (C_i'^{+} + C_i'^{-}) \times (X_i^{\mathrm{T}+} + X_i^{\mathrm{T}-}), \tag{6}$$

where $C_i'^{+}$ and $C_i'^{-}$ are the positive and negative values of C_i'. X_i^{+} and X_i^{-} are the positive and negative values of X_i. The ReLU activation function was adopted, and the input information X_i received by OIU is all positive. The formula can be simplified as

$$Y = \sum_{i=1}^{3} C_i' \times X_i^{\mathrm{T}} = \sum_{i=1}^{3} (C_i'^{+} + C_i'^{-}) \times X_i^{\mathrm{T}} =$$

$$\sum_{i=1}^{3} (C_i'^{+} \times X_i^{\mathrm{T}} - |C_i'^{-}| \times X_i^{\mathrm{T}}) = Y^{+} - |Y^{-}|, \tag{7}$$

where $|C_i'^{-}|$ is the absolute value of $C_i'^{-}$. We implement $C_i'^{+}$ and $|C_i'^{-}|$ by OIU (shown in Fig.2(b)). The data is collected by a PD and subtracted in the electrical field, and then the negative value's operation result is saved.
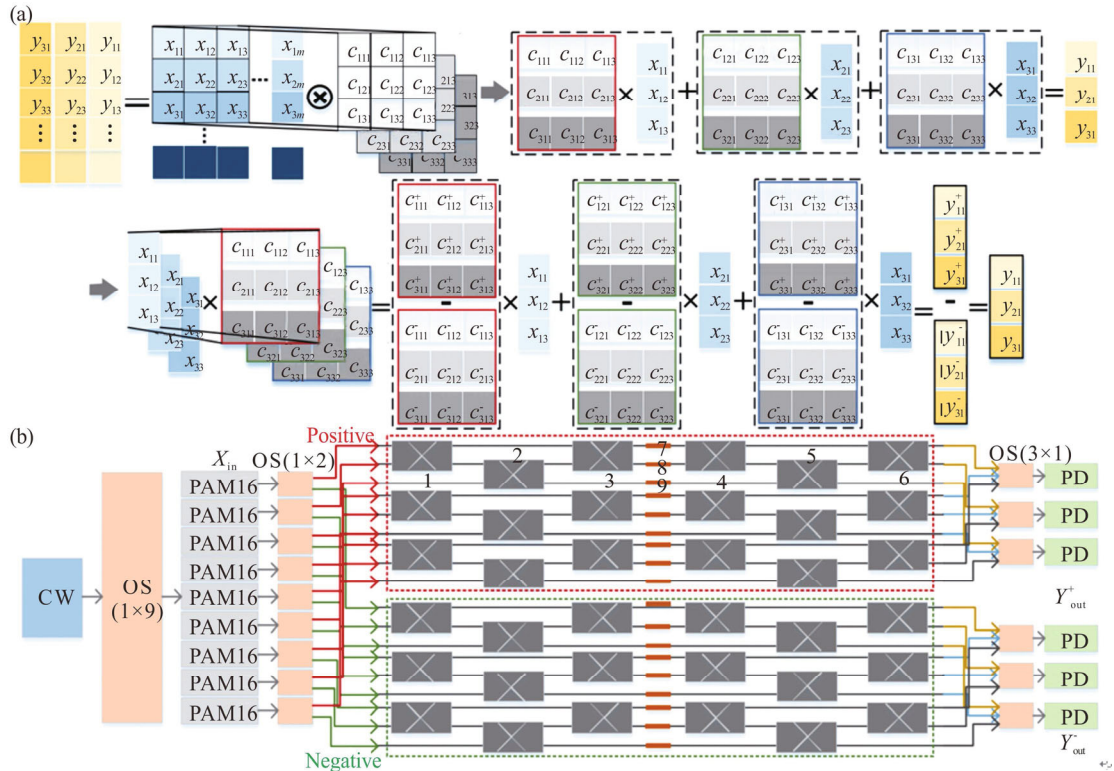
Fig.2 (a) Photonics convolution kernel optimized logic (The three convolution kernels' *i*th row converts into a new 3×3 matrix C_i', which is decomposed into C_i^{+} and $|C_i^{-}|$, and the positive and negative channels run separately); (b) Illustration of optical interference unit

The resolution of PD and phase encoding limit the

recognition precision. Phase encoding noise (σ_φ) and PD

noise (σ_D) are randomly perturbed with a Gaussian distribution. As depicted in Fig.3, different network training accuracies are obtained with different σ_φ and σ_D, realized by the transfer matrix method in the INTERCONNECT (Lumerical). The basic parameters are set as follows.

For the optical source, wavelength is 1 550 nm, power is 18 mW, and half-height width is 20 pm. For the detector, response wavelength is 1 550 nm, and the dark current is 20 nA.

Then, a suitable bit of voltage resolution per channel can be chosen. The output data from OIU is activated by the ReLU function and followed by an FCL and SOFTMAX activation function. Here, FPGA implements the nonlinear transformation $E_{out}=f(E_{in})$, followed by ARAM caching and reorganizing. Then, E_{out} injects into the next stage of the optical amplitude modulator. FPGA calls OIU repeatedly. Thus, the whole network can be realized by only two OIUs.

It is challenging to achieve all-optical CNNs. Here, FPGA implements nonlinearity and data storage. Such hybrid architecture has more straightforward implementation and on-chip integration. The optical convolution kernel is optimized in the calculation process, which retains the negative result and amplifies the optical calculation's efficiency.

(a)

(b)
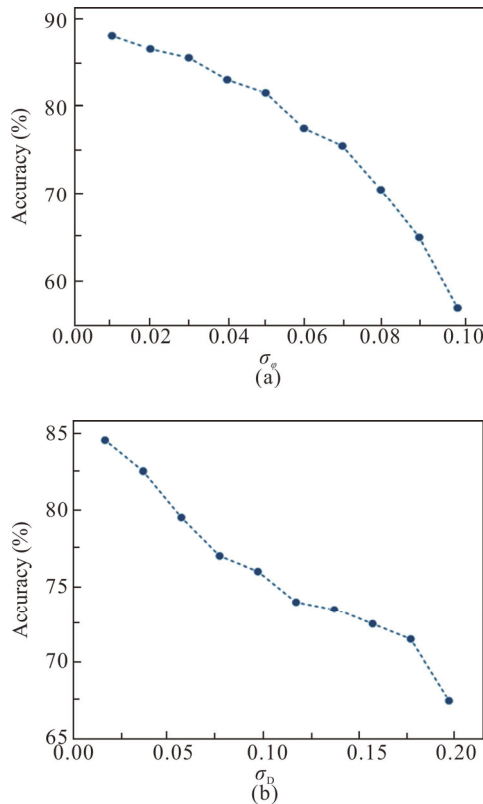
Fig.3 (a) The accuracy of network with various phase encoding errors σ_φ; (b) The accuracy of network with various PD errors σ_D

The overall accuracy rate is limited by σ_φ and σ_D. Simulation results are plotted in Fig.3. The classification accuracy of the network is 89%, when an error distribution is $\sigma_\varphi \leq 0.01$. The $\sigma_\varphi =0.01$ corresponds to an 8-bit accuracy in the phase setting. The classification accuracy of the network is 85%, when an error distribution is $\sigma_D \leq 0.02$. The $\sigma_D =0.02$ corresponds to the dark current of PD of 20 nA. Accuracy rate and confusion matrix of the OHCNN for the Fashion-MNIST dataset are show in Fig.4. Accuracy comparison of single-channel network and two-channel network is shown in Fig.4(c). The accuracy of two-channel network is 87.4%, which is 7.5% higher than that of the single-channel network. It is similar to NVDIA Tesla P100[13]. To alleviate the network's complexity, we could focus on researching lightweight neural networks and binary neural networks suitable for small-scale OIU in the future.

The working speed of OHCNN (S_{OHCNN}) is limited by analog-to-digital converter/digital-to-analog converter ADC/DAC (used on PAM16) speed. In Ref.[9], the power of ADC/DAC (used on PAM16, P_{P_ADC}) is about 200 mW, when its speed is 5 GHz. We used multiplication and accumulation (MAC) to measure the operating performance of OHCNN. Tera floating-point operations per second can be calculated according to $TFlops= MAC \times S_{OHCNN} \times 10^{-12}$. We estimate the energy consumption of the system to be dominated by the OIU's ADC ($P_{O\_ADC}=0.026$ W)[5], the OIU's optical modulators ($P_{O\_MOD} \approx 3$ μW, which can be negligible), the ADC/DAC used on PAM16 ($P_{P\_ADC}=0.1$ W)[5], the optical modulators in PAM16 ($P_{P\_MOD}=0.2$ W)[14], PD ($P_{PD}=0.2$ W)[15], optical source (P_{OS}), and thermal stabilization (P_{TS}). The EER is $TFlops/P_{total}$, where P_{total} is the total energy consumption of the system.

$$EER = \frac{TFlops}{P_{total}} =$$

$$\frac{TFlops}{P_{total\_PAM} + P_{total\_MZI} + P_{total\_PD} + P_{TS} + P_{OS}}, \quad (8)$$

$$P_{total\_PAM} = (P_{P\_MOD} + P_{P\_ADC}) \times n_{PAM} \times 4, \quad (9)$$

$$P_{total\_MZI} = P_{O\_ADC} \times n_{MZI} \times 2, \quad (10)$$

$$P_{total\_PD} = P_{PD} \times n_{PD}, \quad (11)$$

where n_{PAM}, n_{MZI} and n_{PD} are the numbers of PAM16s, MZIs and PDs, respectively. The n_{PAM}, n_{MZI}, n_{PD}, P_{TS} and P_{OS} in single-channel network and two-channel network are shown in Tab.1.

The $TFlops$, P_{total} and EER of NVDIA Tesla P100[13] in single-channel network and two-channel network are shown in Tab.2. The EER of this work is 0.022 3 $TFlops$/W, which is 46.7% higher than that of single-channel network and is 2.53 times of that of NVDIA Tesla P100.

The power consumption is proportional to the number of convolution cores. Simultaneously, the transformation between the optical and electric signals with electronic circuits would increase the total power consumption. Nonlinear activation can be completed in the optical domain[16]. The data can be directly transferred to the next layer without photoelectric conversion, reducing power consumption.

(a)

(b)

(c)
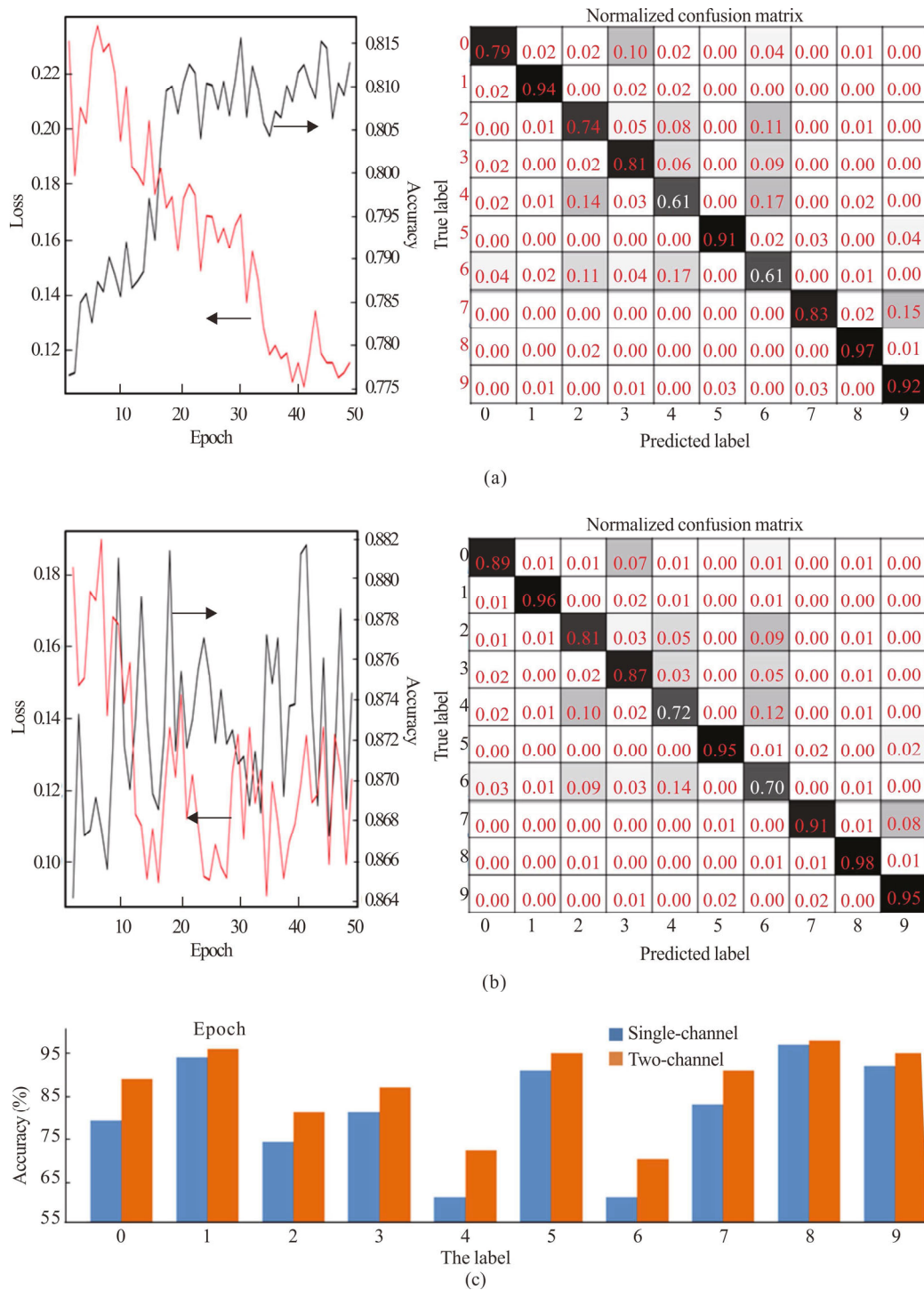
Fig.4 Accuracy, loss and confusion matrix of the OHCNN for the Fashion-MNIST dataset: (a) Single-channel convolution kernel network; (b) Optimized two-channel convolution kernel network; (c) Accuracy comparison of single-channel network and two-channel network

Tab.1 n_{PAM}, n_{MZI}, n_{PD}, P_{TS} and P_{OS} in single-channel network and two-channel network

	n_{PAM}	n_{MZI}	n_{PD}	P_{TS} (W)	P_{OS} (W)
Single-channel	9	27	3	4	0.009
Two-channel	9	54	6	8	0.018

Tab.2 *TFlops*, P_{total} and *EER* of NVDIA Tesla P100, single-channel network and two-channel network

	TFlops	P_{total} (W)	*EER* (*TFlops*/W)
NVDIA	2.65	300	0.008 8
Single-channel	255×10⁻³	16.81	0.015 2
Two-channel	510×10⁻³	22.83	0.022 3

In this paper, we used the optical-electronic hybrid

setup mode to realize CNN. The OIU, composed of MZIs array, performs multiplication and accumulation operations. The convolution kernel layer is split and re-organized, and FPGA encodes and modulates its weight. The convolution kernel is expanded from single-channel to two-channel, containing positive and negative weights. Here, FPGA realizes nonlinear activation, data scheduling and storage, phase encoding, and modulation. The power consumption is proportional to the number of convolution cores. The Fashion-MNIST dataset is used to test the optimized two-channel convolution kernel network architecture's accuracy. The accuracy is 87.4%, which is 7.5% higher than that of the single-channel convolution kernel network. The *EER* of this work is 0.022 3 *TFlops*/W, which is 46.7% higher than that of single-channel network. It needs to be emphasized that the power consumption related to data movement is still an urgent challenge in the current neural network architecture. It is necessary to explore optical nonlinear and optical interconnection to realize all-optical computation.

Statements and Declarations

The authors declare that there are no conflicts of interest related to this article.

References

[1]   LI S, SUN K, LUO Y, et al. Novel CNN-based AP2D-net accelerator: an area and power efficient solution for real-time applications on mobile FPGA[J]. Electronics, 2020, 9(5): 832.

[2]   WU Y, ABDEL-ATY M, ZHENG O, et al. Automated safety diagnosis based on unmanned aerial vehicle video and deep learning algorithm[J]. Transportation research record: journal of the transportation research board, 2020, 2674(99): 036119812092580.

[3]   PENG H, NAHMIAS M A, THOMAS F, et al. Neuromorphic photonic integrated circuits[J]. IEEE journal of selected topics in quantum electronics, 2018, 24(6): 1-15.

[4]   SHEN Y, HARRIS N C, SKIRLO S, et al. Deep learning with coherent nanophotonic circuits[J]. Nature

photonics, 2017, 11: 441-446.

[5]   BANGARI V, MARQUEZ B A, MILLER H, et al. Digital electronics and analog photonics for convolutional neural networks (DEAP-CNNs)[J]. IEEE journal of selected topics in quantum electronics, 2020, 26(1): 1-13.

[6]   ONG J R, OOI C C, ANG T Y L, et al. Photonic convolutional neural networks using integrated diffractive optics[J]. IEEE journal of selected topics in quantum electronics, 2020, 26(5): 1-8.

[7]   PAI S, BARTLETT B, SOLGAARD O, et al. Matrix optimization on universal unitary photonic devices[J]. Physical review applied, 2019, 11: 064044.

[8]   YING Z F, FENG C H, ZHAO Z, et al. Electronic-photonic arithmetic logic unit for high-speed computing[J]. Nature communications, 2020, 11: 2154.

[9]   XU X, ZHU L, ZHUANG W, et al. Photoelectric hybrid convolution neural network with coherent nanophotonic circuits[J]. Optical engineering, 2021, 60(11): 117106.

[10]   CLEMENTS W R, HUMPHREYS P C, METCALF B J, et al. An optimal design for universal multiport interferometers[J]. Optica, 2016, 3(12): 1460.

[11]   RECK M, ZEILINGER A, BERNSTEIN H J, et al. Experimental realization of any discrete unitary operator[J]. Physical review letters, 1994, 73(1): 58-61.

[12]   CONNELLY M J. Semiconductor optical amplifiers[M]. Berlin, Heidelberg: Springer Science & Business Media, 2007.

[13]   CORPORATION N. NVIDIA TESLA V100[EB/OL]. (2018-01-26) [2021-12-04]. https: //www.nvidia.com/ en-us/data-center/tesla-v100/.

[14]   MILLER D A B. Device requirements for optical interconnects to silicon chips[J]. Proceedings of the IEEE, 2009, 97(7): 1166-1185.

[15]   FELDMANN J, YOUNGBLOOD N, KARPOV M, et al. Parallel convolutional processing using an integrated photonic tensor core[J]. Nature, 2021, 589: 52-58.

[16]   JHA A, HUANG C, PRUCNAL P R. Reconfigurable all-optical nonlinear activation functions for neuromorphic photonics[J]. Optics letters, 2020, 45(17): 4819-4822.